Editors' Suggestion

Observation of the Orbital Rashba-Edelstein Magnetoresistance

Shilei Ding,[1] Zhongyu Liang,[1] Dongwook Go,[2,3] Chao Yun,[1] Mingzhu Xue,[1] Zhou Liu,[1] Sven Becker,[3] Wenyun Yang,[1] Honglin Du,[1] Changsheng Wang,[1] Yingchang Yang,[1] Gerhard Jakob,[3,4] Mathias Kläui,[3,4,5] Yuriy Mokrousov,[2,3] and Jinbo Yang[1,6,7,*]

[1]*State Key Laboratory for Mesoscopic Physics, School of Physics, Peking University, Beijing 100871, People's Republic of China*
[2]*Peter Grünberg Institut and Institute for Advanced Simulation, Forschungszentrum Jülich and JARA, 52425 Jülich, Germany*
[3]*Institute of Physics, Johannes Gutenberg-University Mainz, Staudingerweg 7, 55128 Mainz, Germany*
[4]*Graduate School of Excellence Materials Science in Mainz, 55128 Mainz, Germany*
[5]*Center for Quantum Spintronics, Department of Physics, Norwegian University of Science and Technology, NO-7491 Trondheim, Norway*
[6]*Collaborative Innovation Center of Quantum Matter, Beijing 100871, People's Republic of China*
[7]*Beijing Key Laboratory for Magnetoelectric Materials and Devices, Beijing 100871, People's Republic of China*

(Received 13 May 2021; revised 6 December 2021; accepted 7 January 2022; published 10 February 2022)

We report the observation of magnetoresistance (MR) that could originate from the orbital angular momentum (OAM) transport in a permalloy (Py)/oxidized Cu (Cu^*) heterostructure: the orbital Rashba-Edelstein magnetoresistance. The angular dependence of the MR depends on the relative angle between the induced OAM and the magnetization in a similar fashion as the spin Hall magnetoresistance. Despite the absence of elements with large spin-orbit coupling, we find a sizable MR ratio, which is in contrast to the conventional spin Hall magnetoresistance which requires heavy elements. Through Py thickness-dependence studies, we conclude another mechanism beyond the conventional spin-based scenario is responsible for the MR observed in Py/Cu^* structures—originated in a sizable transport of OAM. Our findings not only suggest the current-induced torques without using any heavy elements via the OAM channel but also provide an important clue towards the microscopic understanding of the role that OAM transport can play for magnetization dynamics.

DOI: 10.1103/PhysRevLett.128.067201

The spin-orbit coupling (SOC) plays a critical role in the field of spin orbitronics, leading to various mechanisms for electrical generation of spins such as bulk spin Hall effect [1,2] and interfacial Rashba-Edelstein effect [3–5]. In the scenario of the spin Hall or Rashba-Edelstein effects, a pure spin current or nonequilibrium spin accumulation, whose spin polarization is transverse to the charge current, can be generated in materials with strong bulk SOC or at the interface with the Rashba-type SOC. Vice versa, a charge current can be generated from the spin current via the reciprocal processes, which can be used for the electrical detection of spin [2,6–10]. In the past years, it has been uncovered that the interplay of the direct and inverse spin Hall effects leads to an intriguing flavor of magnetoresistance (MR), commonly referred to as the spin Hall magnetoresistance (SMR) [3,11–13]. The physics behind the SMR is the spin current reflection and absorption via spin-orbit torques (SOTs). It is often assumed that this spin-related MR requires strong SOC [11,12]. Within this paradigm, however, one would not expect that a light metal like Cu with negligible SOC could play a significant role in the generation of SOTs or SMR.

Recently, it has been predicted that the orbital angular momentum (OAM) can be electrically induced at the surface or interface [14–19] via a process called the orbital Rashba-Edelstein effect [15,20–22]. Despite its similarity to the spin counterpart, it is independent of SOC and the inversion symmetry breaking alone is sufficient for its emergence. If the SOC is taken into consideration, the chiral OAM texture couples to the spin angular momentum, leading to the coexistence of the spin and orbital Rashba-Edelstein effects [19]. Importantly, recent experiments indicate that the natural oxidation of Cu can lead to large SOTs [23–26], which supports the idea that the OAM can be electrically generated without heavy elements [25–27]. The surface of the naturally oxidized Cu is electrically insulating and the interface between the metallic ferromagnetic layer $(FM)/CuO_x$ is considered vital for the effect [24]. One of the proposed mechanisms is that the OAM can be electrically induced by the orbital Rashba-Edelstein effect at the surface of the CuO_x, and the OAM is injected into the adjacent FM, where the OAM interacts with the local magnetic moment via the SOC [19,28]. In principle, a combination of the so-called orbital torque and its

reciprocal process can result in a SMR-like effect, which originates in the OAM rather than the spin angular momentum. However, to date, there is still a lack of reports on the MR originating from the nonequilibrium OAM induced by the orbital Rashba-Edelstein effect, which we refer to as the orbital Rashba-Edelstein MR (ORMR).

In this Letter, we report the observation of the ORMR in the Py/oxidized Cu (denoted by Cu* hereafter) bilayer system. The angular dependence of the MR depends on the relative angle between the induced OAM and the magnetization in a similar fashion as the SMR. While the SMR requires heavy elements with large SOC, however, our system does not contain any heavy elements. By varying the thickness of the Cu* layer we confirm that the MR originates from the interface. Through Py thickness dependence studies, we can ascertain the *effective* spin relaxation length of Py in Py/Cu* diverges from the value in Py/Pt. From this, we can deduce whether spin transport alone plays a role, thus identifying to what extent OAM is responsible for the observed results.

All samples are prepared by pulsed laser deposition and the Hall bar devices with a line width of 75 μm are achieved during the deposition process with the help of a shadow mask. The fabricated Cu films are kept in the air for 48 h before transport measurements to obtain naturally oxidized Cu films (Cu*). The 3 nm thick Cu* is electrically insulating indicating the full oxidization of Cu. On the other hand, the 7 nm thick Cu* stays conducting, which means that the oxygen concentration gradient is within 7 nm and there exists a Cu/CuO_x mixture for the 7 nm Cu*. As a metallic FM layer, we use Py ($Ni_{81}Fe_{19}$). Details on the deposition conditions can be found in the Supplemental Material [29].

We first measure the angular dependence of the MR in Py(5)/Cu*(3) sample by rotating the direction of the applied field $\mu_0\boldsymbol{H}$ in xy plane (α scan), yz plane (β scan), and zx plane (γ scan) as shown in Fig. 1. The applied field strength is set to 6 T, which is large enough to saturate the magnetization (M_s) along the $\mu_0\boldsymbol{H}$ direction and we observe a sizable MR in all three orthogonal planes. The α and γ scan MR ratios are consistent with the prediction of the anisotropic MR of the Py layer, where the $Cu^*(3) = CuO_x(3)$ is insulating, and the applied charge current flows in the Py layer. Note that $\alpha = 0°$ and $\gamma = 90°$ correspond to the identical physical situation with magnetic field and current directions parallel. The anisotropic MR phenomenology of polycrystalline FM predicts $\rho_{xx} = \rho_\perp + (\rho_\parallel - \rho_\perp)m_x^2$ [35], where $\rho_\parallel$ and $\rho_\perp$ are the resistivity when the magnetization direction $\boldsymbol{m}$ aligns along and perpendicular to the charge current direction, m_x is the x component of $\boldsymbol{m} = \boldsymbol{M}/M_s$. This predicts that the variations of the resistivity in the α and γ scans follow $[\Delta\rho_{xx}(\alpha)/\rho_{xx}(\alpha)] \sim \cos^2\alpha$ and $[\Delta\rho_{xx}(\gamma)/\rho_{xx}(\gamma)] \sim \sin^2\gamma$, which are consistent with the data shown in Figs. 1(c) and 1(c), respectively.

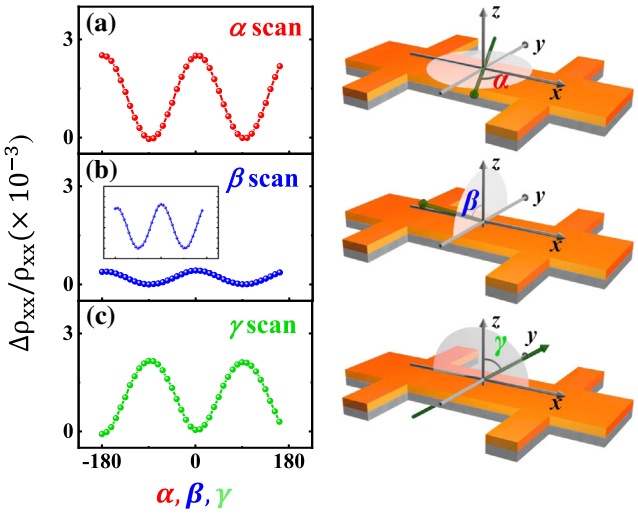

FIG. 1. (a)–(c) The angular dependent MR measurements in Py(5)/Cu*(3) heterostructure at 300 K and 6 T in the three $\mu_0\boldsymbol{H}$-rotation planes (α, β, γ). The schematics on the right show the sample Hall bar and the definition of the axes, angles, and measurement configuration. $\Delta\rho_{xx}/\rho_{xx}$ is the MR ratio collected in different $\mu_0\boldsymbol{H}$-rotation planes. The inset in (b) shows a zoom for the MR signal in the yz plane.

However, the anisotropic MR cannot explain the MR obtained in the β scan, where we find $[\Delta\rho_{xx}(\beta)/\rho_{xx}(\beta)] \sim \cos^2\beta$ as shown in Fig. 1(b). The observed MR in the β scan exhibits a similar angular dependence as the SMR scenario, where the resistivity is given by $\rho_{xx} = \rho_0 - \rho_1 m_y^2$. Here ρ_0 is the resistivity offset, ρ_1 is the magnitude of the resistivity change. Considering the negligible SOC of Cu*, a conventional SMR cannot lead to the novel MR in the β scan. Also, the spin current is believed not to be the origin of SOT in Py/Cu* heterostructures [26], and thus the spin Rashba-Edelstein MR cannot explain the result. From the above considerations, we argue that the ORMR is the most plausible mechanism for the observed MR in the β scan. At the interface of Py(5)/Cu*(3), the inversion symmetry is broken and the orbital asymmetry leads to the orbital Rashba effect [19]. Analogous to the "spin" Rashba effect that can induce the spin current [36], the orbital Rashba effect results in the chiral OAM texture in $\mathbf{k}$ space, and the application of an external electric field $\boldsymbol{E}$ leads to induced OAM along the direction of $\hat{\boldsymbol{z}} \times \boldsymbol{E}$. The induced OAM can flow along z and be absorbed by the FM. The orbital current can be understood as a wave packet consisting of an orbital-polarized state such as $d_{xy} \pm id_{yz}$, which can be induced by an external electric field even under a strong crystal field [37,38]. The mechanism of the ORMR is schematically illustrated in Fig. 2. When the magnetization is perpendicular to the direction of the induced OAM (blue circles with orange circular arrows), the OAM can be absorbed into the FM as it couples to the spin via the SOC and exerts a torque [28] [Fig. 2(a)]. In contrast, when the magnetization is parallel to the direction of the induced

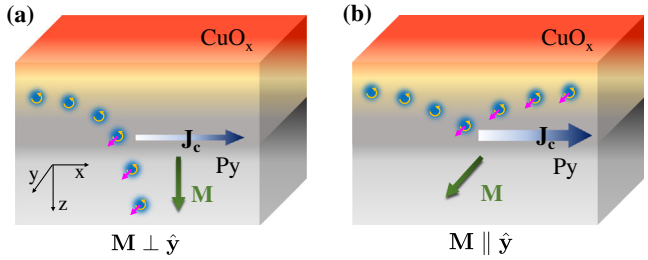

FIG. 2. Schematic illustration of the ORMR. As the charge current flows at the interface to the insulating CuO_x along x, the y component of the OAM (blue circle with orange circular arrow) is induced by the orbital Rashba-Edelstein effect due to the inversion symmetry breaking caused by the oxygen gradient. (a) When the direction of the magnetization (green arrow) is perpendicular to the direction of the induced OAM, the OAM is absorbed by the FM (Py) as it exerts a torque on the magnetization via the SOC that entangles the OAM with the spin (magenta arrow). (b) When the magnetization direction is parallel to the direction of the OAM, the OAM is reflected from the interface. Therefore, (a) exhibits higher resistivity compared to (b).

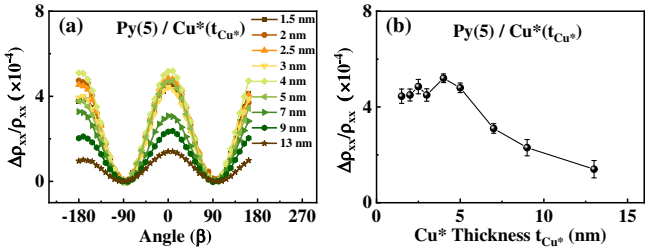

FIG. 3. (a) Angular dependence of the ORMR for $Py(5)/Cu^*(t_{Cu^*})$ samples with different Cu^* layer thicknesses. (b) ORMR ratio $\Delta\rho_{xx}/\rho_{xx}$ as a function of the thickness of Cu^*. The MR ratio keeps nearly constant for $t_{Cu^*} \leq 5$ nm, indicating a typical interfacial mechanism. For $t_{Cu^*} > 5$ nm, the MR ratio decreases monotonically as the thickness of Cu^* increases.

OAM, the OAM is reflected from the interface as it cannot exert torque [Fig. 2(b)]. As a result, the configuration in Fig. 2(a) has higher resistance as compared to the configuration in Fig. 2(b). We remark that the angular dependences of the orbital torque and the spin-injection torque are qualitatively similar, and so are the angular dependences of the ORMR and SMR.

To further understand the properties of the observed ORMR, we carry out Cu^* thickness-dependent measurements. Figure 3(a) presents the β scan MR of $Py(5)/Cu^*(t_{Cu^*})$ for various Cu^* thicknesses t_{Cu^*}. Note that while the magnitudes differ, all the samples follow the SMR-like angular dependence $[\Delta\rho_{xx}(\beta)/\rho_{xx}(\beta)] \sim \cos^2\beta$. We extract the MR ratio by $(\Delta\rho_{xx}/\rho_{xx}) = [\rho_{xx}(\beta = 0°) - \rho_{xx}(\beta = 90°)]/\rho_{xx}(\beta = 90°)$ for each sample, showing the t_{Cu^*} dependence of the MR ratio in Fig. 3(b). When the thickness of t_{Cu^*} is below 5 nm, the naturally oxidized Cu is electrically insulating and the MR ratio stays nearly constant, highlighting that the ORMR originates in the Py/Cu^* interface. For thicker Cu^* samples ($t_{Cu^*} > 5$ nm), we find a monotonic decrease of the MR as t_{Cu^*} increases which is induced either by the current shunting due to low resistivity of Cu or by the blocking of the orbital current in non-oxidized Cu in which the $3d$ shell is fully occupied. We note that the oxygen gradient is crucial for the ORMR as the electronic configuration of Cu^* becomes d^8 or d^9 instead of d^{10}, which can mediate the orbital current. If a Py layer is adjacent to the CuO_x, the OAM is absorbed by the magnetization, however, when the Cu^* is thicker than the length scale of the oxygen gradient (~5 nm), the orbital current cannot efficiently penetrate through the nonoxidized Cu due to intrinsic quenching of the OAM since the pure Cu without oxidization has negligible d orbital character close to the Fermi energy [19]. We note that similar behavior was also observed in the measurement of the orbital torque in $AlO_x/Cu/CoFe$, where the decrease of the torque efficiency seems to be much more drastic than the current shunting effect [27], which indicates suppression of the orbital transport in nonoxidized Cu.

To identify the origin of the ORMR and compare it to the conventional SMR, we next study the FM thickness dependence of the ORMR in comparison with the SMR in Py/Pt. The angular dependence of the SMR in $Py(t_F)/Pt(4)$ and the ORMR $Py(t_F)/Cu^*(3)$ are shown in Figs. 4(a) and 4(b), respectively, for various thicknesses of t_F. From these data, we plot the thickness dependences of the SMR in $Py(t_F)/Pt(4)$ and the ORMR $Py(t_F)/Cu^*(3)$ as a function of t_F in Figs. 4(c) and 4(d), respectively. For $Py(t_F)/Pt(4)$ samples, the SMR ratio exhibits a peak at ~3 nm and decreases for thicker Py samples. While the increase of the SMR for $t_F < 3$ nm is due to the spin dephasing in Py, the decrease for thicker Py is due to the current shunting. We note that our result is similar to the previous studies [39,40]. For the quantitative analysis, we use the diffusion model developed by Kim *et al.* [13], which takes into account the charge current shunting and the *longitudinal* spin current diffusing into the FM in magnetic bilayers. According to this model, the SMR is given by

$$\frac{\Delta\rho_{xx}}{\rho_{xx}} \sim \theta_{\mathrm{eff}}^2 \frac{\lambda_N}{t_N} \frac{\tanh^2(t_N/2\lambda_N)}{1+\xi} \left[\frac{g_R}{1 + g_R \coth(t_N/2\lambda_N)} - \frac{g_F}{1 + g_F \coth(t_N/2\lambda_N)} \right],$$
$$g_R = 2\rho_N \lambda_N \mathrm{Re}[G_{\mathrm{mix}}],$$
$$g_F = (1 - P^2) \frac{\rho_N \lambda_N}{\rho_F \lambda_F} \tanh(t_F/\lambda_F), \quad (1)$$

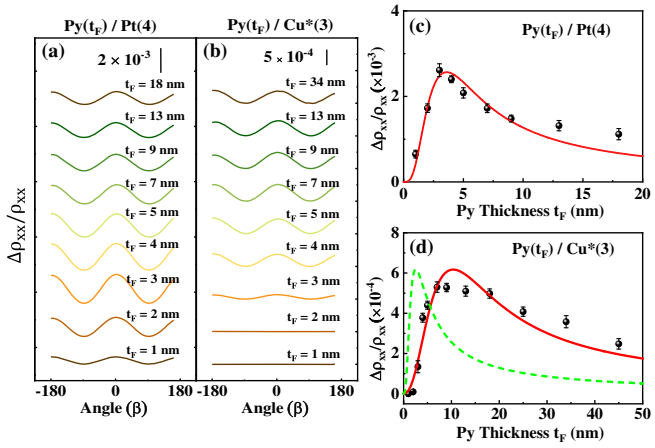

FIG. 4. (a) and (b) The ORMR measurements in the β scan for Py(t_F)/Pt(4) and Py(t_F)/Cu*(3) at 6 T. (c) and (d) The plots of the Py thickness dependence of the MR ratio $(\Delta\rho_{xx}/\rho_{xx})$ taken from (a) and (b), respectively. The red curves are the fitting curves of the data. The green dashed curve in (d) is the fitting by forcing the effective relaxation length of Py to match the value taken from the Py/Pt samples, which shows a significant deviation from the obtained data.

where t_N, ρ_N, λ_N, and $\theta_{\rm eff}$ represent the thickness, resistivity, spin diffusion length, and the effective spin Hall angle of nonmagnetic metal, $G_{\rm mix}$ is the spin-mixing conductance at the interface, ρ_F, λ_F, and P refer to the resistivity, spin diffusion length, and spin polarization of the FM layer, respectively. Here, $\xi = (\rho_N t_F/\rho_F t_N)$ reflects the current shunting effect. If we consider the spin dephasing in the FM, $\theta_{\rm eff}$ is given by [41]

$$\theta_{\rm eff} = \theta_{\rm SH}[1 - {\rm sech}(t_F/\lambda_{\rm eff})], \tag{2}$$

where $\theta_{\rm SH}$ is the saturated spin Hall angle, $\lambda_{\rm eff}$ is the effective length required for the spin absorption in the FM. In order to reduce the number of free parameters in the fitting, we replace λ_F by $\lambda_{\rm eff}$ in Eq. (1), which allows us to extract the parameters in a more reliable manner. The fitting of the thickness dependence of the SMR is shown with a red curve in Fig. 4(c). We assume $\rho_F = \rho_F^{\rm bulk}(1 + C_F^{\rm int}/t_F)$, where $\rho_F^{\rm bulk} = (8.0 \pm 0.8) \times 10^{-7}\,\Omega$m and $C_F^{\rm int} = (2.5 \pm 0.5) \times 10^{-9}$ m are extracted by fitting ρ_F measured for different values of t_F [29]. On the other hand, we find that the resistivity of Pt stays nearly constant with respect to the change of t_N, so we assume $\rho_N = 1.2 \times 10^{-6}\ \Omega$m. The rest of the parameters are assumed: ${\rm Re}[G_{\rm mix}] = 1.0 \times 10^{15}\ \Omega^{-1}\,{\rm m}^{-2}$ for the Py/Pt interface [13], $P = 0.49$ for Py [42], and $\lambda_N = 1.5$ nm in Pt. From the fitting, we obtain $\lambda_{\rm eff} = 1.4 \pm 0.1$ nm and $\theta_{\rm SH} = 0.28 \pm 0.01$. The extracted value of $\theta_{\rm SH}$ in Pt may seem relatively large. However, considering that the SMR is caused by a complicated process involving the interplay between spin absorption and reflection at the interface, the inaccuracy in the determination of $\theta_{\rm SH}$ is not too surprising. Nonetheless, we find that the extracted value of $\lambda_{\rm eff}$ is much less affected by the choice of the parameters.

The overall behavior of the Py thickness dependence of the ORMR in Py(t_F)/Cu* (3) is similar to that of the SMR in Py(t_F)/Pt(4). However, the maximum MR ratio appears when Py is thicker than 7 nm, which is much larger than the value measured in Py(t_F)/Pt(4). Meanwhile, the MR ratio decreases for larger values of Py thickness due to the current shunting. To understand the difference of the peak positions for the maximum ORMR and that for the SMR, we develop a spin diffusion model for interface/FM systems, whose derivation can be found in the Supplemental Material [30]. It is given by

$$\frac{\Delta\rho_{xx}}{\rho_{xx}} \sim \lambda_{\rm int}^2[1 - {\rm sech}(t_F/\lambda'_{\rm eff})]^2\left[\frac{2\rho_F\lambda'_{\rm eff}{\rm Re}[G_{\rm mix}] - (1-P^2)\tanh(t_F/\lambda'_{\rm eff})}{\lambda'_{\rm eff}t_F}\right], \tag{3}$$

where $\lambda_{\rm int}$ describes the efficiency of the spin current generation from the interface, which has the dimension of a length. Most importantly, $\lambda'_{\rm eff}$ is the length over which the injected OAM is absorbed in Py. By assuming ${\rm Re}[G_{\rm mix}] = 0.5 \times 10^{15}\ \Omega^{-1}\,{\rm m}^{-2}$ [43] and $P = 0.49$ [42] for the fitting in Fig. 4(d), we find $\lambda'_{\rm eff} = 4.8 \pm 0.3$ and $\lambda_{\rm int} = 0.11 \pm 0.01$ nm. We remark that $\lambda'_{\rm eff} \approx 5$ nm extracted from Py/Cu* is significantly different from $\lambda_{\rm eff} \approx 1.4$ nm extracted from Py/Pt. If the microscopic mechanisms for the angular momentum transfer share the same origin, i.e., spin injection, $\lambda'_{\rm eff}$ should be comparable to $\lambda_{\rm eff}$. If we force $\lambda'_{\rm eff} = \lambda_{\rm eff}$ in Eq. (3), the fitting curve significantly deviates from the data (green dashed curve). This leads to the conclusion that the origin of the MR in Py(t_F)/Cu*(3) is not the conventional spin mechanism due to the spin Hall effect or spin Rashba-Edelstein effect and indicates that the MR is rooted in the OAM dynamics, where the orbital torque or the orbital-to-spin current conversion should be considered.

We note that we have introduced only one length scale $\lambda'_{\rm eff}$ in the analysis of the ORMR. This is a simplification of the mechanism which involves the orbital injection, orbital-to-spin conversion, and their reciprocal processes, and there is no guarantee that the length scales responsible for each process are identical. Thus, $\lambda'_{\rm eff}$ should be understood as an effective value that results from the interplay among different processes. Characterization of individual microscopic processes is one of the most important tasks in the

field of spin-orbitronics. Clarifying the role of individual processes should serve as the aim of future efforts, which goes beyond the scope of this work.

We remark that long-range propagation of the OAM due to distinct mechanism of the angular momentum transfer has been theoretically predicted [44], which is much larger than the spin dephasing length. Nonetheless, other possible mechanisms have been discussed such as the spin-vorticity coupling [45]. However, the interpretation of the spin-vorticity coupling eventually predicts that the spin current is injected into the FM, which cannot explain the FM thickness dependence. A discussion of other possible mechanisms can be found in Ref. [25]. We believe that the ORMR may be experimentally observed in other systems which do not contain heavy elements. We note that the orbital torque has been observed in many other systems as well, especially in bulk materials where the orbital Hall effect is pronounced [46–48].

In conclusion, we report a magnetoresistance effect in Py/naturally oxidized Cu bilayers at room temperature. This effect cannot be explained by conventional SMR due to the absence of any heavy element with large SOC, and we term this ORMR. By varying the thickness of the oxidized Cu layer, we find that the mechanism originates from the interface, indicating the orbital Rashba-Edelstein effect. Careful examination of the Py thickness dependence shows that the spin diffusion and spin dephasing lengths significantly deviate from the values measured in conventional Py/Pt bilayers. This strongly suggests that the conventional spin-injection mechanism cannot serve as the microscopic origin of the MR observed in Py/naturally oxidized Cu bilayers, supporting the ORMR scenario. Our findings not only unambiguously demonstrate the current-induced torque without using any heavy element via the OAM channel but also provide an important clue towards the microscopic understanding of the interaction of the out-of-equilibrium OAM and magnetization in magnetic materials. The results of our work point to an exciting possibility that low-SOC materials can be efficiently used for the transport of orbital angular momentum with much higher efficiency than that associated with the transport of spin, which might prove to be crucial in taking the next step from conventional spintronics to orbitronics that can be realized without expensive and environmentally harmful heavy metal materials.

We acknowledge the support from the National Key Research and Development Program of China (Grants No. 2017YFA0206303, No. 2016YFB0700901, No. 2017YFA0403701). National Natural Science Foundation of China (Grants No. 51731001, No. 11675006, No. 11805006, No. 11975035), Graduate School of Excellence Materials Science in Mainz (MAINZ, GSC266), Deutsche Forschungsgemeinschaft (DFG, German Research Foundation) Spin+X (A01, A11, B02) TRR 173–268565370 and Project No. 358671374. The work was further supported by the Horizon 2020 Framework Programme of the European Commission under FETOpen Grant Agreement No. 863155 (s-Nebula) and the European Research Council Grant Agreement No. 856538 (3D MAGiC) and the Research Council of Norway through its Centers of Excellence funding scheme, project number 262633 "QuSpin."

S. D., Z. L., and D. G. contributed equally to this work.

*Corresponding author.
jbyang@pku.edu.cn

[1] A. Manchon, J. Železný, I. M. Miron, T. Jungwirth, J. Sinova, A. Thiaville, K. Garello, and P. Gambardella, Rev. Mod. Phys. **91**, 035004 (2019).
[2] J. Sinova, S. O. Valenzuela, J. Wunderlich, C. H. Back, and T. Jungwirth, Rev. Mod. Phys. **87**, 1213 (2015).
[3] H. Nakayama, Y. Kanno, H. An, T. Tashiro, S. Haku, A. Nomura, and K. Ando, Phys. Rev. Lett. **117**, 116602 (2016).
[4] V. M. Edelstein, Solid State Commun. **73**, 233 (1990).
[5] J. C. R. Sánchez, L. Vila, G. Desfonds, S. Gambarelli, J. P. Attané, J. M. De Teresa, C. Magén, and A. Fert, Nat. Commun. **4**, 2944 (2013).
[6] L. Wang, R. J. H. Wesselink, Y. Liu, Z. Yuan, K. Xia, and P. J. Kelly, Phys. Rev. Lett. **116**, 196602 (2016).
[7] K. Shen, G. Vignale, and R. Raimondi, Phys. Rev. Lett. **112**, 096601 (2014).
[8] X. Fan, H. Celik, J. Wu, C. Ni, K.-J. Lee, V. O. Lorenz, and J. Q. Xiao, Nat. Commun. **5**, 3042 (2014).
[9] E. Saitoh, M. Ueda, H. Miyajima, and G. Tatara, Appl. Phys. Lett. **88**, 182509 (2006).
[10] W. Zhang, M. B. Jungfleisch, W. Jiang, J. E. Pearson, and A. Hoffmann, J. Appl. Phys. **117**, 17C727 (2015).
[11] H. Nakayama, M. Althammer, Y. T. Chen, K. Uchida, Y. Kajiwara, D. Kikuchi, T. Ohtani, S. Geprags, M. Opel, S. Takahashi, R. Gross, G. E. W. Bauer, S. T. B. Goennenwein, and E. Saitoh, Phys. Rev. Lett. **110**, 206601 (2013).
[12] Y.-T. Chen, S. Takahashi, H. Nakayama, M. Althammer, S. T. B. Goennenwein, E. Saitoh, and G. E. W. Bauer, Phys. Rev. B **87**, 144411 (2013).
[13] J. Kim, P. Sheng, S. Takahashi, S. Mitani, and M. Hayashi, Phys. Rev. Lett. **116**, 097201 (2016).
[14] S. R. Park, C. H. Kim, J. Yu, J. H. Han, and C. Kim, Phys. Rev. Lett. **107**, 156803 (2011).
[15] D. Go, J.-P. Hanke, P. M. Buhl, F. Freimuth, G. Bihlmayer, H.-W. Lee, Y. Mokrousov, and S. Blügel, Sci. Rep. **7**, 46742 (2017).
[16] V. Sunko, H. Rosner, P. Kushwaha, S. Khim, F. Mazzola, L. Bawden, O. J. Clark, J. M. Riley, D. Kasinathan, M. W. Haverkort, T. K. Kim, M. Hoesch, J. Fujii, I. Vobornik, A. P. Mackenzie, and P. D. C. King, Nature (London) **549**, 492 (2017).
[17] J.-H. Park, C. H. Kim, H.-W. Lee, and J. H. Han, Phys. Rev. B **87**, 041301 (2013).
[18] M. Ünzelmann, H. Bentmann, P. Eck, T. Kißlinger, B. Geldiyev, J. Rieger, S. Moser, R. C. Vidal, K. Kißner, L. Hammer, M. A. Schneider, T. Fauster, G. Sangiovanni, D. Di Sante, and F. Reinert, Phys. Rev. Lett. **124**, 176401 (2020).

[19] D. Go, D. Jo, T. Gao, K. Ando, S. Blügel, H.-W. Lee, and Y. Mokrousov, Phys. Rev. B **103**, L121113 (2021).

[20] T. Yoda, T. Yokoyama, and S. Murakami, Nano Lett. **18**, 916 (2018).,

[21] L. Salemi, M. Berritta, A. K. Nandy, and P. M. Oppeneer, Nat. Commun. **10**, 5381 (2019).

[22] A. Johansson, B. Göbel, J. Henk, M. Bibes, and I. Mertig, Phys. Rev. Research **3**, 013275 (2021).

[23] X. Qiu, K. Narayanapillai, Y. Wu, P. Deorani, D. H. Yang, W. S. Noh, J. H. Park, K. J. Lee, H. W. Lee, and H. Yang, Nat. Nanotechnol. **10**, 333 (2015).

[24] H. An, Y. Kageyama, Y. Kanno, N. Enishi, and K. Ando, Nat. Commun. **7**, 13069 (2016).

[25] S. Ding, A. Ross, D. Go, L. Baldrati, Z. Ren, F. Freimuth, S. Becker, F. Kammerbauer, J. Yang, G. Jakob, Y. Mokrousov, and M. Kläui, Phys. Rev. Lett. **125**, 177201 (2020).

[26] Y. Tazaki, Y. Kageyama, H. Hayashi, T. Harumoto, T. Gao, J. Shi, and K. Ando, arXiv:2004.09165.

[27] J. Kim, D. Go, H. Tsai, D. Jo, K. Kondou, H.-W. Lee, and Y. C. Otani, Phys. Rev. B **103**, L020407 (2021).

[28] D. Go and H.-W. Lee, Phys. Rev. Research **2**, 013177 (2020).

[29] See Supplemental Material at http://link.aps.org/supplemental/10.1103/PhysRevLett.128.067201 for the details about the deposition conditions, and transport measurement, the magnetic properties of Py, the field dependence of ORMR ratio for $\mathrm{Py}(3)/\mathrm{Cu}^{*}(3)$, and $\mathrm{Py}(4)/\mathrm{Cu}^{*}(3)$, the field dependence of ORMR for $\mathrm{Py}(t_F)/\mathrm{Pt}(4)$, and $\mathrm{Py}(t_F)/\mathrm{Cu}^{*}(3)$, MR in yz plane scan for the single Py layer, the field dependence of ORMR for $\mathrm{Py}(5)/\mathrm{Cu}^{*}(3)$, the fitting details for the Py thickness dependence of ORMR ratio, and the resistivity for $\mathrm{Py}(t_F)/\mathrm{Pt}(4)$ and $\mathrm{Py}(t_F)/\mathrm{Cu}^{*}(3)$, which includes Refs. [13,30–34].

[30] S. Ding, R. Wu, J. B. Fu, X. Wen, H. L. Du, S. Q. Liu, J. Z. Han, Y. C. Yang, C. S. Wang, D. Zhou, and J. B. Yang, Appl. Phys. Lett. **107**, 172404 (2015).

[31] S. Vélez, V. N. Golovach, A. Bedoya-Pinto, M. Isasa, E. Sagasta, M. Abadia, C. Rogero, L. E. Hueso, F. S. Bergeret, and F. Casanova, Phys. Rev. Lett. **116**, 016603 (2016).

[32] H. Ochoa, R. Zarzuela, and Y. Tserkovnyak, J. Magn. Magn. Mater. **538**, 168262 (2021).

[33] P. Wang, S. W. Jiang, Z. Z. Luan, L. F. Zhou, H. F. Ding, Y. Zhou, X. D. Tao, and D. Wu, Appl. Phys. Lett. **109**, 112406 (2016).

[34] M. DC, R. Grassi, J.-Y. Chen, M. Jamali, D. Reifsnyder Hickey, D. Zhang, Z. Zhao, H. Li, P. Quarterman, Y. Lv, M. Li, A. Manchon, K. A. Mkhoyan, T. Low, and J.-P. Wang, Nat. Mater. **17**, 800 (2018).

[35] T. McGuire and R. Potter, IEEE Trans. Magn. **10**, 1109–1138 (1975).

[36] V. P. Amin, J. Zemen, and M. D. Stiles, Phys. Rev. Lett. **121**, 136805 (2018).

[37] D. Go, D. Jo, H.-W. Lee, M. Kläui, and Y. Mokrousov, Europhys. Lett. **135**, 37001 (2021).

[38] D. Go, D. Jo, C. Kim, and H.-W. Lee, Phys. Rev. Lett. **121**, 086602 (2018).

[39] Y. Yang, Y. Xu, K. Yao, and Y. Wu, AIP Adv. **6**, 065203 (2016).

[40] S.-Y. Huang, H.-L. Li, C.-W. Chong, Y.-Y. Chang, M.-K. Lee, and J.-C.-A. Huang, Sci. Rep. **8**, 108 (2018).

[41] Y. Wang, P. Deorani, X. Qiu, J. H. Kwon, and H. Yang, Appl. Phys. Lett. **105**, 152412 (2014).

[42] T. Kimura, T. Sato, and Y. Otani, Phys. Rev. Lett. **100**, 066602 (2008).

[43] Y. Liu, Z. Yuan, R. J. H. Wesselink, A. A. Starikov, and P. J. Kelly, Phys. Rev. Lett. **113**, 207202 (2014).

[44] D. Go, D. Jo, K.-W. Kim, S. Lee, M.-G. Kang, B.-G. Park, S. Blügel, H.-W. Lee, and Y. Mokrousov, arXiv:2106.07928.

[45] G. Okano, M. Matsuo, Y. Ohnuma, S. Maekawa, and Y. Nozaki, Phys. Rev. Lett. **122**, 217701 (2019).

[46] Y-G. Choi, D. Jo, K-H. Ko, D. Go, K-H. Kim, H-G. Park, C. Kim, B-C. Min, G-M. Choi, and H-W. Lee, arXiv:2109.14847.

[47] D. Lee, D. Go, H.-J. Park, W. Jeong, H.-W. Ko, D. Yun, D. Jo, S. Lee, G. Go, J. H. Oh, K.-J. Kim, B.-G. Park, B.-C. Min, H. C. Koo, H.-W. Lee, O. Lee, and K.-J. Lee, Nat. Commun. **12**, 6710 (2021).

[48] S. Lee, M.-G. Kang, D. Go, D. Kim, J.-H. Kang, T. Lee, G.-H. Lee, J. Kang, N. J. Lee, Y. Mokrousov, S. Kim, K.-J. Kim, K.-J. Lee, and B.-G. Park, Commun. Phys. **4**, 234 (2021).